Chapter 5. Evaporation and discharge dynamics of highly charged two-component droplets generated by electrospray ionization

5.1. Abstract

We report studies of the Rayleigh discharge dynamics of charged two-component droplets consisting principally of methanol with either 2-methoxyethanol, *tert*-butanol, or *m*-nitrobenzyl alcohol. Phase Doppler anemometry (PDA) characterizes droplets generated by electrospray ionization according to size, velocity, and charge as they move through a uniform, linear electric field within an ion mobility cell. Repeated field reversals allow multiple PDA measurements of selected micron-sized droplets with up to 10^7 elementary positive charges. This "ping-pong" technique generates individual droplet histories from which we ascertain solvent evaporation behavior and the dynamics of mass and charge loss to progeny droplets during Rayleigh discharge events. On average, methanol discharges at 127% its Rayleigh limit and releases 25% of its net charge. Binary methanol droplets containing up to 50% *tert*-butanol discharge at a lower point than pure methanol and release a greater fraction of their net charge. Interestingly, methanol / *tert*-butanol droplets evaporate at a similar rate to pure methanol. Droplets of methanol / 2-methoxyethanol release a greater portion of their net charge as the fraction of 2-methoxyethanol in the droplets increase. These droplets evaporate at a rate similar to that of pure 2-methoxyetanol droplets. Mixed 99% methanol / 1% *m*-nitrobenzyl

alcohol droplets possess discharge characteristics similar to methanol, however 2% *m*-nitrobenzyl droplets evaporate down to a fixed size and charge that remains constant with no observable discharges. We compare these results to previous experiments, and discuss implications for the use of binary solvents in electrospray and field-induced droplet ionization mass spectrometry.

5.2. Introduction

Multi-component solvent systems are common in the electrospray mass spectrometry of biomolecules, yet questions remain regarding the mechanisms by which different solvent systems yield unique spectra of otherwise identical analytes. Electrospray ionization[1-3] is a popular tool in mass spectrometry because of its ability to generate low-energy, multiply charged biomolecules and molecular clusters.[4] In the electrospray process, an applied electric field induces charge separation in a solution flowing from a capillary needle. The resulting electrohydrodynamic forces draw the liquid to a point referred to as the Taylor cone that sprays a fine mist of charged droplets.[5] Mass spectrometric applications utilize the subsequent evaporation and discharge processes that ultimately yield desolvated gas phase ions or clusters. Despite the popularity of the technique, recent experiments present conflicting results regarding the dynamics and mechanisms involved.

Our current understanding of charged droplet instability and breakup begins with the seminal work of Lord Rayleigh. In 1882, he proposed that the repulsive force due to the net surface charge destabilizes the natural mode oscillations within a droplet. He postulated that the natural oscillation of a droplet becomes unstable when the net charge,

q, on a droplet of radius r and surface tension σ exceeds a critical value, q_R, given by eq (5.1).

$$q_R = 8\pi\varepsilon^{1/2}\sigma^{1/2}r^{3/2} \quad (5.1)$$

In (5.1), ε is the permittivity of the surrounding medium. He suggests the droplet emits fine jets of charged progeny when q exceeds q_R, but his analysis does little else to describe the dynamics of the event. Significant research has been performed to elucidate these mechanisms. In the consensus view, solvent evaporates from a highly charged micron-sized droplet until $q > q_R$ at which point the droplet distorts and emits jets of small, highly charged progeny droplets. The progeny droplets are typically 1-10% the diameter of the parent droplet. This Rayleigh discharge event has been visually confirmed showing one jet from methanol[6] and *n*-heptane[7] and two jets from ethylene glycol droplets.[8] Discharge events typically release 10 to 40% of a droplet's net charge but only 1 to 5% of a droplet's mass.[4]

In the nanometer size regime, researchers propose two competing mechanisms for discharge events. Dole's original charge residue model (CRM) suggests the process of evaporation and Rayleigh discharge-like events continues until the formation of desolvated ions.[9] Iribarne and Thomson propose the ion evaporation model (IEM) where the surface electric field due to excess charge is sufficient to desorb ions directly from the surface of the nanodroplet.[10]

Recent mass spectrometry studies of analytes dissolved in multi-component solvents have had profound implications for the understanding of these evaporation and discharge mechanisms. Williams and co-workers note a correlation between solution surface tension and the charge-state distribution of electrosprayed polymers and

biomolecules in the gas-phase. Terming the phenomenon "supercharging," they note the addition of *m*-nitrobenzyl alcohol ($\sigma \sim 0.050$ N m^{-1}) significantly increases the charge state distributions of poly(ethylene glycol) dendrimers sprayed from methanol ($\sigma = 0.022$ N m^{-1}) yet decreases the charge state distribution of the dendrimers sprayed from water ($\sigma = 0.072$ N m^{-1}).[11-13] In contrasting experiments, Samalikova and Grandori report no change in the charge state distribution of denatured proteins upon the addition of *n*-propanol ($\sigma = 0.072$ N m^{-1}) to aqueous solutions.[14] The conflicting results suggest that more research is necessary to understand the processes that govern charging of analytes in electrospray mass spectrometry. Such studies motivate the present investigation.

We report the evaporation and discharge dynamics of ten binary solvent systems comprised of methanol with either *tert*-butanol, 2-methoxyethanol, or *m*-nitrobenzyl alcohol, shown in Table 5.1. Discharges are characterized by measuring the droplet diameter and charge, the charge lost in the event, and the charge as a function of the Rayleigh limit at the time of the event. Binary droplet evaporation is compared to the single-component evaporation model discussed in Chapter Three. Concisely, evaporation of micron-sized droplets is dominated by the rate at which vapor diffuses away from the droplet surface. Equation (5.2) determines the evaporation rate for single-component droplets.[15]

$$\frac{d}{dt} d_{\mathrm{p}} = \frac{-4 D_{ij}\left(T_{\mathrm{p}}\right) M}{R \rho_{\mathrm{p}} d_{\mathrm{p}}} \frac{p_{\mathrm{p}}\left(T_{\mathrm{p}}\right)}{T_{\mathrm{p}}} \tag{5.2}$$

In eq (5.2), solvent-specific parameters include $D_{ij}(T_{\mathrm{p}})$, the temperature-dependent diffusivity of solvent vapor *i* in gas *j*, solvent molar mass *M*, droplet density ρ_{p}, and

equilibrium vapor pressure, $p_p(T_p)$, at equilibrium surface temperature T_p, while R is the gas constant. The equilibrium surface temperature is depressed relative to the ambient temperature, T_∞, because evaporation is spontaneous yet endothermic. Equation (5.2) is simplified from a more rigorous model in which solvent vapor in the ambient gas inhibits evaporation. Experimentally, a constant flow of dry nitrogen gas washes through the apparatus flushing solvent vapor allowing this simplification. Integrating the evaporation rate yields eq (5.3).

$$d_p^2 = d_o^2 + st \tag{5.3}$$

Thus a plot of d_p^2 versus time is linear with intercept d_o^2 and slope s containing the solvent-specific parameters given by eq (5.4). Spontaneous evaporation is endothermic, lowering the surface temperature below that of the ambient gas.

$$s = -\frac{8D_{ij}(T_p)M}{R\rho_p}\frac{p_p(T_p)}{T_p} \tag{5.4}$$

Evaporation models of multicomponent droplets require solving the equations for heat and mass transfer at the droplet-gas interface as well as the diffusion through the liquid and convective diffusion of the solvent vapor in air. Diffusion through the liquid is generally orders-of-magnitude slower than diffusion through air suggesting the presence of concentration gradients within the droplet. This is confirmed by calculating the Biot number, Bi, which is the ratio of the time scale for self-diffusion in the liquid to the time scale of convective diffusion of the solvent molecules in air. Following a derivation similar Clark, eq (5.5) estimates the Biot number for the evaporation of methanol from a pure, 40 μm diameter droplet.[16] In eq (5.5), k_c represents the mass transfer coefficient under Stokes flow and is given by eq (5.6).

$$\mathrm{Bi} = \frac{d_p k_c}{2D_{ij}} \tag{5.5}$$

$$k_c = \frac{D_{ij}}{2a}\left[0.92 + 0.991(\mathrm{Sc}\ \mathrm{Re})^{1/3}\right] \tag{5.6}$$

In eq (5.6), Re is the Reynolds number and Sc is the Schmidt number. For methanol, D_{ij} = 0.13 cm^2 s^{-1}, Sc = 1.13, and Re ~ 0.2 at the terminal settling speed of a 40 μm diameter droplet. As a result, Bi ~ 5000 indicating the time scale of internal diffusion is significantly greater than the time scale of external, convective diffusion.

There are no exact solutions for the general case of binary droplet evaporation. As a result, models of multi-component evaporation frequently employ simplifying assumptions. Davis et al. study low vapor pressure oils that evaporate nearly isothermally.[17-20] Simplified models accurately predict the evaporation behavior of these oils. For the volatile solvents considered in this study, quasi-steady state models approximate the evaporation dynamics. In quasi-steady state evaporation, droplets exposed to air initially undergo a period of unsteady evaporation while the surface temperature decreases to an equilibrium value.[21] At the equilibrium temperature depression, a binary droplet evaporates at a "constant composition mixture."[22] In other words, the composition of the droplet is said to be in a quasi-steady state. The rate of evaporation in this state is proportional to the droplet surface area. Thus eq (5.3) models the droplet size, however *s* becomes a multi-component function of bulk parameters for both components as well as the activity coefficients for the two-component system. We compare the binary component slopes, *s*, from a linear regression of d_p^2 versus *t* to the corresponding values for pure droplets of the component species.

5.3. Experimental Section

Rather than use an electrodynamic balance, where the electric forces balance the force of gravity to trap and hold droplets, we employ an ion mobility spectrometer (IMS). In our IMS, $qE \neq mg$ and droplets are dragged through a linear electric field while being characterized according to size, equilibrium velocity, and net charge using a phase Doppler anemometer (PDA).

Chapter Three describes the ping-pong apparatus and equations of motion in detail. Only deviations and specific implementations are discussed. Briefly, the instrument consists of three parts: the electrospray source that generates charged droplets in the 10-100 μm size range, the mobility cell (often referred to as a drift cell or the drift region), and a phase Doppler anemometer (PDA) that characterizes droplet size, velocity and charge. An electric field initially directs positively charged droplets upward through the cell. When the PDA detects a droplet, the electric field reverses and droplets travel downward through the cell. Repeated field reversals cause the detected droplet to "ping-pong" through the measurement volume providing a temporal profile of droplet size, velocity, and charge for that droplet. Following this acquisition, the field resets so that droplets travel upwards for the analysis of another droplet. Typically, highly charged droplets take ~200 ms to travel the 10 cm distance between the electrospray source and the PDA measurement volume, and are subsequently characterized every 10 ms.

The methanol (HPLC grade, EM Science), glycerol (99.5%, EM Science), *tert*-butanol (99%, Sigma Aldrich), 2-methoxyethanol (98%, Sigma Aldrich), and *m*-nitrobenzyl alcohol solvents were used without further purification. The electrospray needle was held 2 mm from the first aperture in the IMS and maintained at 850 V for neat

methanol and between 900 and 1150 V for the binary solvent systems. In each case, solution flow rates were 0.5 – 2 mL min^{-1} and dry nitrogen gas flowed downward through the cell at 0.3 L min^{-1} or 0.6 cm s^{-1}. The voltages, needle positions, and flow rates resulted in a metastable electrospray of micron-sized droplets. Higher voltages and electric fields result in cone-jet electrosprays that generate droplets too small for detection by the PDA.

5.4. Results

Binary systems consisting of methanol / 2-methoxyethanol, methanol / *tert*-butanol, and 99% methanol / 1% *m*-nitrobenzyl alcohol showed Rayleigh discharge phenomena. These droplets were initially 30-50 μm in diameter and generally carried a nascent charge of 60-90% q_R from the electrospray source. Droplets consisting of 98% methanol / 2% *m*-nitrobenzyl alcohol showed no discharge events but rather evaporated to down to a size and charge that remained constant for up to 500 ms. These droplets were initially 5-20 μm in diameter with a nascent charge of 40-60% q_R. Because of their different behavior, binary systems showing Rayleigh discharge are presented and discussed separately from the 98% methanol / 2% *m*-nitrobenzyl alcohol droplets.

5.4.1. Droplets with observed Rayleigh discharge events

Figure 5.1 shows a representative history for a single droplet of 75% methanol and 25% 2-methoxyethanol undergoing multiple Rayleigh discharges. When first characterized, the droplet is roughly 32 μm in diameter (frame A) with ~4.2×10^6 elementary charges (C). This corresponds to roughly 95% the Rayleigh limit for

methanol (D). In repeated observations through 0.2 s, the droplet's diameter decreases and the speed (B) increases. The speed increase is due to the constant electrical force, qE, becoming proportionally greater than the force of gravity $m_p g$, which is decreasing as the droplet loses mass to evaporation. The small oscillations in speed are due to the droplet traveling upwards against gravity more slowly than traveling downward with gravity. We attribute the diameter oscillations to the change in the relative refractive index between droplets traveling upwards through dry gas and droplets traveling downwards through solvent-saturated gas.

During the first 0.2 seconds of acquisition, the charge remains constant (C) and the percent Rayleigh limit (D) increases due to constant charge and decreasing size. At 0.2 s after the initial characterization, the charge decreases suddenly resulting in a decrease in velocity and the percent Rayleigh limit. Conversely, there is no significant decrease in mass loss at this time. We interpret this sudden charge loss to be a Rayleigh discharge event. The droplet presented in Figure 5.1 shows six such discharges represented by arrows.

Discharge dynamics are classified according to charge loss and the percent Rayleigh limit. The change in average charge between discharge events classifies the charge loss as shown by dotted lines in Figure 5.1C. The percent Rayleigh limit at discharge is simply the last recorded value before the sharp decrease characteristic of a discharge event.

Evaporation dynamics are described by a slope of diameter squared versus time as computed by a linear regression and residual plots of the regressions show no trend. The dotted curve in Figure 5.1A demonstrates this fit corresponding to $s \sim 1200\ \mu m^2\ s^{-1}$.

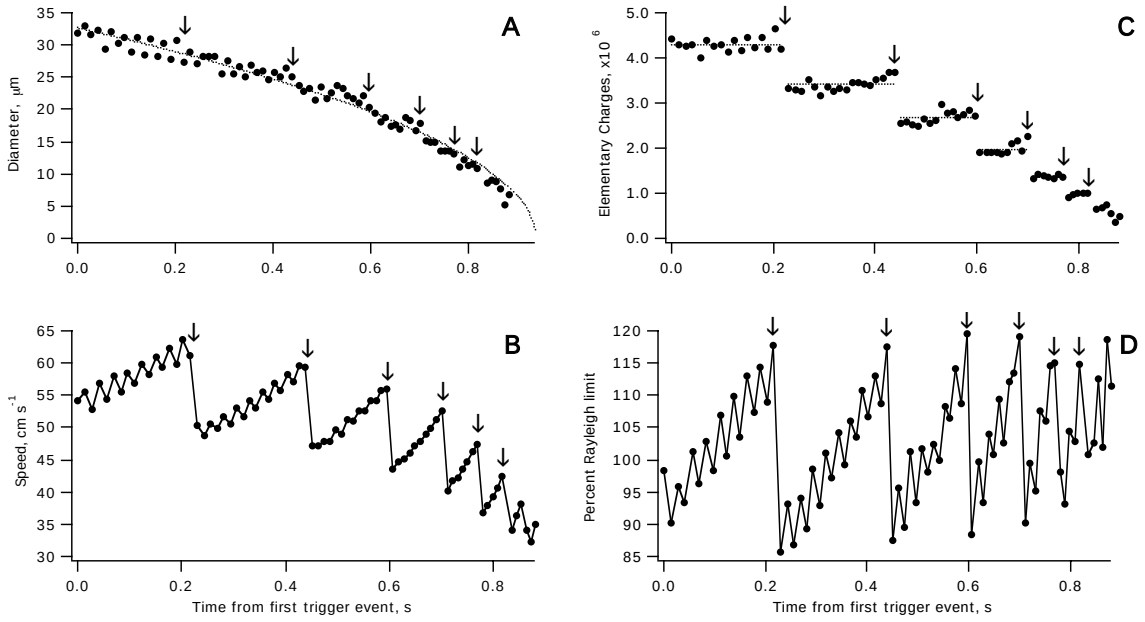

Figure 5.1. Acquired history of a 75% methanol 25% 2-methoxyethanol droplet including size (A), velocity (B), charge (C), and percent Rayleigh limit (D). As the droplet evaporates, its speed increases and charge stays constant until a discharge event. The six observed events (indicated by arrows) occur at ~120% the Rayleigh limit for methanol and are characterized by loss of ~25% of the droplet charge and an undetectable mass loss.

Table 5.1 summarizes the charge loss and evaporation characteristics of the nine binary systems showing Rayleigh discharge events. Previous results for single-component droplets of hydrocarbon solvents *n*-heptane, *n*-octane, and *p*-xylene[23] and of traditional electrospray solvents methanol, water, and acetonitrile,[24] show no correlation between droplet size and the percent charge lost in a Rayleigh discharge event. Binary droplets do demonstrate a correlation as is illustrated in Figure 5.2 for methanol / *tert*-butanol, in Figure 5.3 for methanol / 2-methoxyethanol, and in Figure 5.4 for 99% methanol / 1% *tert*-butanol. In each of these binary systems, smaller droplets eject a larger percent of their net charge than the larger droplets. As a result of the size – charge loss correlation, the average charge loss values reported in Table 5.1 are not rigorous but rather serve as a rapid summary of the Rayleigh discharge phenomena for binary systems.

Percent Rayleigh limit data for the binary systems is reported as the percent Rayleigh limit of methanol because the droplet composition is not known *a priori*. The unknown density and refractive index each introduce a small ~5% error in the diameter and charge assignments, however the unknown surface tension prohibits an exact determination of q_R by eq (5.1) and the percent Rayleigh limit at a discharge event. For all binary systems, surface tension is taken as bulk methanol value, $\sigma = 0.022$ N m^{-1}. All other components have $\sigma > 0.022$ N m^{-1} so computed q_R values are a *lower* bound and the reported percent Rayleigh limit at discharge, $100\% \times q/q_R$, in Table 5.1 and Figures Figure 5.2 through Figure 5.4 represents an *upper* bound.

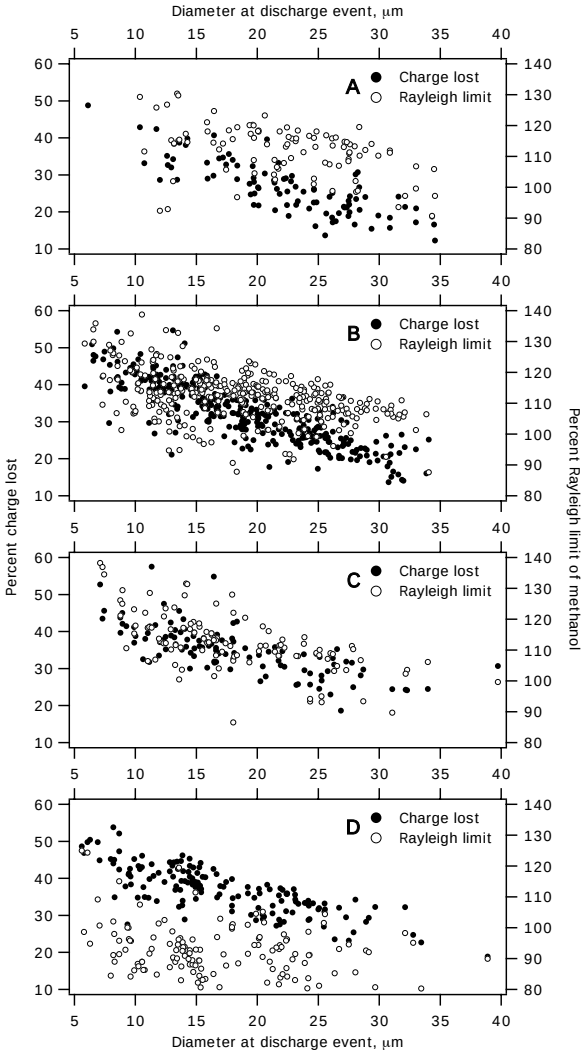

Figure 5.2. Percent charge lost (closed circle) and percent Rayleigh limit (open circles) versus the diameter at discharge for 5% (A), 10% (B), 25% (C) and 50% (D) *tert*-butanol droplets. The distribution in each system shows a dependence on droplet size with larger droplets ejecting less of their net charge than the smaller droplets.

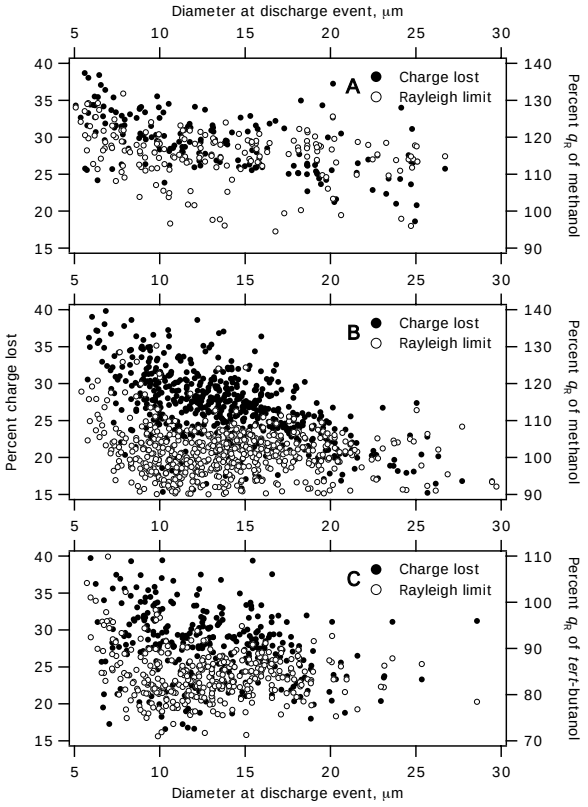

Figure 5.3. Percent charge lost (closed circle) and percent Rayleigh limit (open circles) versus the diameter at discharge for 25% (A), 50% (B), and 100% (C) 2-methoxyethanol droplets. The distribution in each the binary systems (A) and (B) shows a dependence on droplet size while pure 2-methoxyethanol (C) shows no correlation between charge loss and droplet size.

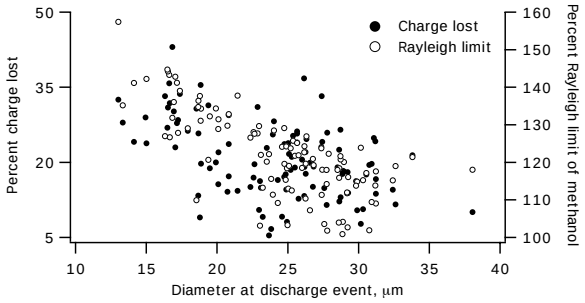

Figure 5.4. Percent charge lost (closed circle) and percent Rayleigh limit (open circles) versus the diameter at discharge for 99% methanol / 1% *m*-nitrobenzyl alcohol droplets. The distribution in each system shows a dependence on droplet size with larger droplets ejecting less of their net charge than the smaller droplets.

5.4.2. Droplets with no Rayleigh discharge events

Droplets of 98% methanol / 2% *m*-nitrobenzyl alcohol show no Rayleigh discharge events, but rather evaporation down to a size that remained fixed for the duration of the characterization. Figure 5.5 shows representative data for a droplet with 2% *m*-nitrobenzyl alcohol. Droplet size (Figure 5.5A) decreases steadily for the first 0.25 s while both the velocity (B) and the percent Rayleigh limit (D) increase consistently with solvent evaporation. For the remainder of the acquisition, all values remain constant. Droplet charge (C) is constant for the entire acquired lifetime of the droplet.

5.5. Discussion

5.5.1. Evaporation dynamics and mass loss in a discharge event

Droplet diameter decreases in time due to solvent evaporation as is evident in Figure 5.1. Within the accuracy of the measurements, no observable additional decrease in size accompanies the discharge events. Based on uncertainties in the diameter measurements, previous studies in our laboratory bound the maximum change in diameter in a Rayleigh discharge event at 4%.[23]

Table 5.1 shows the evaporation of pure methanol droplets (s = -4350 $\mu m^2 s^{-1}$) and pure 2-methoxyethanol droplets (s = -2300 $\mu m^2 s^{-1}$) agree well with the theoretical values. In the case of the methanol / *tert*-butanol droplets, calculated s values are remarkably similar to pure methanol. In contrast, droplets of methanol / 2-methoxyethanol show evaporation rates similar to pure 2-methoxyethanol. In all cases, plots of d^2 are linear with respect to time indicating that eq (5.3) accurately models the droplets, which are undergoing quasi-steady state evaporation.

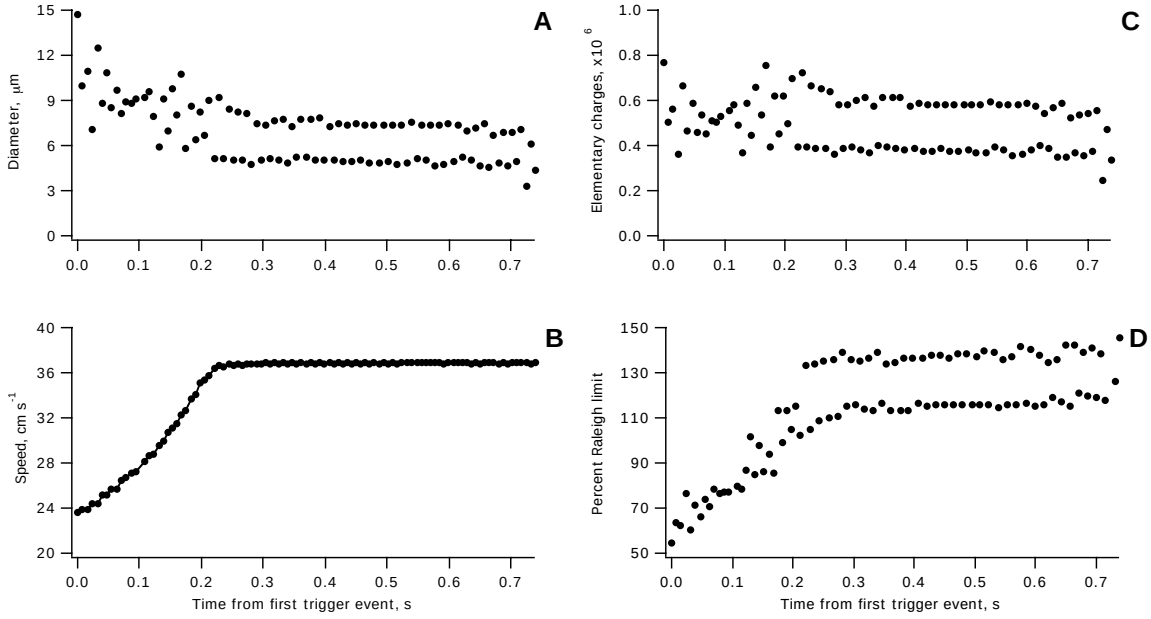

Figure 5.5. Acquired history of a methanol droplet with 2% *m*-nitrobenzyl alcohol. The droplet is initially charged at 50% of its Rayleigh limit and evaporates for ~0.25 s after the initial acquisition. With the droplet no longer evaporating after ~0.25 s, all values remain constant for the remainder of the acquisition sequence.

5.5.2. Correlation between droplet size and charge loss

The percent charge loss for the binary droplets studied is generally between 5 and 40%. When *tert*-butanol and 2-methoxyethanol are added to methanol the percent charge lost in a discharge event increases. Table 5.1 demonstrates that the average charge loss for pure methanol droplets is ~25%, however the addition of *tert*-butanol increases the average charge loss up to ~37%. The surface tension of pure *tert*-butanol is 0.020 N m^{-1} compared to 0.022 N m^{-1} for methanol indicating that surface tension is not a decisive parameter for this change. On the other hand, the addition of 2-methoxyethanol results in a small increase to 27-29% charge lost which is roughly identical to the ~28% charge lost from pure 2-methoxyethanol droplets.

Figure 5.2 through Figure 5.4 show a correlation between the size of the droplet and the percent charge lost in a discharge event. For binary systems, larger droplets consistently lose a lower fraction of their net charge than smaller droplets. For droplets that undergo sequential discharge events such as the droplet in Figure 5.1, we generally observe an average increase of 15%. Previous studies on pure droplets demonstrate that the percent charge loss in an event is roughly proportional to the surface tension of the liquid. Generally, hydrocarbon solvents eject ~18% of their net charge[23], alcohols and glycols eject ~20-30% of their charge,[8,24,25] and water ejects 20-40% of its net charge.[24] The percent of charge lost from droplets of pure solvents is consistent over the range of sizes studied, both in previous investigations,[23,24] and for pure methanol and 2-methoxyethanol in this experiment.

The size dependence of charge loss indicates the physical parameters controlling charge loss are changing as the droplets evaporate and discharge. We attribute this to one

of two possible explanations. First, droplets may not be in a quasi-steady state as they evaporate even though their diameter is well described by (5.3). Future work may address this with a rigorous theoretical treatment regarding the evaporation of the droplets studied in this experiment. The other, more likely, possibility is that the discharge events are disrupting the quasi-steady state evaporation. Before a discharge event, the composition of the surface is significantly different from that of the bulk. As a result, the discharge events remove a small amount of mass from the surface disrupting the steady state and changing the overall physical parameters of the droplet. This too may be simulated through theoretical models of binary droplet evaporation with the periodic removal of surface mass from a simulated, evaporating droplet. This would also predict how the components fractionate between the parent and progeny from a discharge event, which is not measured in this experiment.

5.5.3. Droplets with no Rayleigh discharge events

Droplets of 98% methanol and 2% *m*-nitrobenzyl alcohol show no discharge events, but rather, they evaporate to a constant size and charge. These droplets are generally smaller than other droplets studied and carry significantly lower initial net charge relative to the Rayleigh limit. Droplets initially possess 40-60% the Rayleigh limit of charge and stop evaporating before reaching the 125% q_R point at which methanol droplets undergo Rayleigh discharge in our apparatus.

The small nascent charge results in correspondingly small initial velocities of ~20 cm/s suggesting droplets travel for 500 ms between production and their initial characterization. If the droplets evaporate at $s = -4350\ \mu m^2\ s^{-1}$, the nascent droplet

diameter would be ~60 μm. Thus droplets that "freeze" have lost roughly 90% of their diameter which corresponds to 99.9% volume loss. This indicates that these droplets evaporate to a "core" comprised almost entirely of the low volatility *m*-nitrobenzyl alcohol component.

5.5.4. Implications for electrospray mass spectrometry

Iavarone and Williams suggest that the supercharging phenomenon manifests itself late in the droplet evaporation and discharging process when discharge is explained by the CRM or IEM.[11-13] However, observations of size-dependent charge loss in this experiment indicate that the Rayleigh discharge events of nascent electrospray droplets may have an effect on those droplets. Thus the entire lifetime of evaporation and discharge is important for explaining charge state distributions of analytes of multi-component solutions as well as the supercharging phenomenon.

The Rayleigh discharge dynamics for 99% methanol / 1% *m*-nitrobenzyl alcohol resemble that of pure methanol whereas observations of the 98% / 2% mixture shows profoundly different behavior. This indicates that small changes in the *m*-nitrobenzyl alcohol concentration have a profound impact on droplet dynamics. This agrees well with the supercharging phenomenon which results in a significant change in the charge state distribution of biomolecules and poly(ethylene glycol) dendrimers with the initial addition of 1 to 5% *m*-nitrobenzyl alcohol. Exploring the discharge dynamics of the 98% / 2% system at elevated temperatures and longer acquisitions may reveal the Rayleigh discharge dynamics relevant to electrospray mass spectrometry.

5.6. Conclusions

Understanding the evaporation and discharge dynamics of binary droplets is critical to knowing and controlling the charge state distributions of biomolecules and clusters studied in electrospray mass spectrometry. Many studies demonstrate that the charge state distribution of biomolecules changes depending on the solvent system that is electrosprayed. Studies of Rayleigh discharge in droplets of methanol and *tert*-butanol demonstrate an increase in the charge lost in a discharge event with increasing initial quantities of *tert*-butanol. Conversely, droplets of methanol and 2-methoxyethanol show evaporation and discharge dynamics similar to that of pure 2-methoxyethanol.

Methanol evaporates significantly more rapidly than *m*-nitrobenzyl alcohol. Evaporation of 99% methanol / 1% *m*-nitrobenzyl alcohol shows evaporation and discharge dynamics similar to those of pure methanol, however 98% / 2% droplets show no observable Rayleigh discharge events. Thus small changes in the initial concentrations of *m*-nitrobenzyl alcohol have profound implications for the discharge dynamics and electrospray mass spectrometry.

5.7. Acknowledgements

The authors gratefully acknowledge Dr. J. N. Smith whose experimental designs and insight made the current investigation possible, and Dr. Richard Flagan for his valuable discussions. This material is based on work supported by the National Science foundation under grants CHE-9727566 and CHE-0416381 and support from the Beckman Institute at Caltech.

system	percent charge lost	percent Rayleigh limit*	experim. slope, s ($\mu m^2\ s^{-1}$)
methanol	25 ± 7	127 ± 12	-4350 (-4750)
95% methanol 5% *tert*-butanol	27 ± 7	112 ± 9	-4400
90% methanol 10% *tert*-butanol	32 ± 9	113 ± 9	-4300
75% methanol 25% *tert*-butanol	35 ± 7	113 ± 11	-4400
50% methanol 50% *tert*-butanol	37 ± 7	91 ± 10	-4500
75% methanol 25% 2-methoxyethanol	29 ± 4	116 ± 7	-1500
50% methanol 50% 2-methoxyethanol	27 ± 7	102 ± 13	-2000
100% 2-methoxyethanol	28 ± 7	85 ± 7	-2300 (-1925)
99% methanol 1% *m*-nitrobenzyl alcohol	21 ± 8	123 ± 14	-4500

Table 5.1. Experimental charge loss, percent Rayleigh limit at discharge, and evaporation values for binary systems characterized by the "ping-pong" technique. Evaporation slope values in parenthesis represent calculated values from thermodynamic parameters.

5.8. References

(1) Yamashita, M.; Fenn, J. B. *J. Phys. Chem.* **1984**, *88*, 4451.

(2) Yamashita, M.; Fenn, J. B. *J. Phys. Chem.* **1984**, *88*, 4671.

(3) Fenn, J. B.; Mann, M.; Meng, C. K.; Wong, S. F.; Whitehouse, C. M. *Science* **1989**, *246*, 64.

(4) *Electrospray Ionization Mass Spectrometry*; Cole, R. B., Ed.; John Wiley and Sons: New York, 1997.

(5) Taylor, G. *Proc. R. Soc. London, Ser. A* **1964**, *280*, 383.

(6) Hager, D. B.; Dovichi, N. J.; Klassen, J.; Kebarle, P. *Anal. Chem.* **1994**, *66*, 3944.

(7) Gomez, A.; Tang, K. *Phys. Fluids* **1994**, *6*, 404.

(8) Duft, D.; Atchtzehn, T.; Muller, R.; Huber, B. A.; Leisner, T. *Nature* **2003**, *421*, 6919.

(9) Dole, M.; Mack, L. L.; Hines, R. L.; Mobley, R. C.; Ferguson, L. D.; Alice, M. B. *J. Chem. Phys.* **1968**, *49*, 2240.

(10) Thomson, B. A.; Iribarne, J. V. *J. Chem. Phys.* **1979**, *71*, 4451.

(11) Iavarone, A. T.; Jurchen, J. C.; Williams, E. R. *J. Am. Soc. Mass Spectrom.* **2000**, *11*, 976.

(12) Iavarone, A. T.; Williams, E. R. *Int. J. Mass Spectrom.* **2002**, *219*, 63.

(13) Iavarone, A. T.; Williams, E. R. *J. Am. Chem. Soc.* **2003**, *125*, 2319.

(14) Samalikova, M.; Grandori, R. *J. Am. Chem. Soc.* **2003**, *125*, 13352.

(15) Hinds, W. C. *Aerosol Technology: Properties, Behaivor, and Measurement of Airborne Particles*, 2nd ed.; John Wiley & Sons, Inc.: New York, 1999.

(16) Clark, M. M. *Transport Modeling for Environmental Engineers and Scientists*; Wiley Interscience: New York, 1996.

(17) Ravindran, P.; Davis, E. J. *J. Colloid Interface Sci.* **1982**, *85*, 278.

(18) Buehler, M. F.; Allen, T. M.; Davis, E. J. *J. Colloid and Interface Sci.* **1991**, *146*, 79.

(19) Allen, T. M.; Taflin, D. C.; Davis, E. J. *Ind. Eng. Chem. Res.* **1990**, *29*, 682.

(20) Widmann, J. F.; Davis, E. J. *Aerosol Sci. Technol.* **1997**, *27*, 243.

(21) Newbold, F. R.; Amundson, N. R. *AIChE J.* **1973**, *19*, 22.

(22) Ray, A. K.; Venkatraman, S. *AIChE J.* **1995**, *41*, 938.

(23) Grimm, R. L.; Beauchamp, J. L. *Anal. Chem.* **2002**, *74*, 6291.

(24) Smith, J. N.; Flagan, R. C.; Beauchamp, J. L. *J. Phys. Chem. A* **2002**, *106*, 9957.

(25) Duft, D.; Lebius, H.; Huber, B. A.; Guet, C.; Leisner, T. *Phys. Rev. Lett.* **2002**, *89*, art. no. 084503.